

Resonance and Instability of Blade-Shaft Coupled Bending Vibrations with In-plane Blade Vibration

Norihisa Anegawa¹, Hiroyuki Fujiwara¹, Akira Okabe² and Osami Matsushita¹

¹Department of Mechanical Engineering, National Defense Academy
 1-10-20 Hashirimizu, Yokosuka, Kanagawa, 239-8686, Japan

²Hitachi, Ltd., Automotive Systems
 18-13, Soto-Kanda, 1-chome, Chiyoda-ku, Tokyo, 101-8608, Japan

Abstract

As a major component of a power plant, a turbine generator must have sufficient reliability. Longer blades have lower natural frequency, thereby requiring that the design of the shaft and blade takes into account the coupling of the blade vibration mode, nodal diameter $k=0$ and $k=1$ with vibration of the shaft.

The present work analyzes the coupling of the translation motion of the shaft with in-plane vibration of the blades with $k=1$ modes. At a rotational speed $\Omega_1=|\omega_s-\omega_b|$, the resonance of the blades has a relatively large amplitude. A violent coupled resonance was observed at a rotational speed $\Omega_2=\omega_s+\omega_b$. Resonance in blade vibration at $\Omega_1=|\omega_s-\omega_b|$ was experimentally confirmed.

Keywords: Blade-Shaft coupled vibration, Bending vibration, Resonance, Instability, In-plane vibration, Turbine generator

1. Introduction

As a major component of the power plant, a turbine generator must have sufficient reliability. The rotary shaft system is usually designed to give a low Q-factor and avoid resonance based on the rotor-dynamic analysis of the bending and torsional vibration of the shaft-bearing system, in which the blades are assumed to be a rigid disk. Meanwhile, the blade is designed to avoid resonance under the rated operation conditions based on analysis of a single blade under ideal conditions where the shaft is assumed to be fixed [1],[2].

The long blades used in turbine generators for nuclear power plants have low natural frequencies, thereby necessitating a design that takes into consideration blade-shaft coupled vibration. General conditions for coupling of blade and shaft vibrations are shown in Table 1.

Table1 Blade-shaft coupled vibration

Blade \ Shaft		$k = 0$		$k = 1$	
		in plane	out of plane	in plane	out of plane
Torsion		①	—	—	—
Axial		—	②	—	—
Radial	Translation	—	—	③	—
	Tilting	—	—	—	④

- ① Shaft torsional vibration and blade in-plane vibration with nodal diameter $k=0$
- ② Shaft thrust vibration and blade out-of-plane vibration with nodal diameter $k=0$
- ③ Shaft translation vibration and blade in-plane vibration with nodal diameter $k=1$
- ④ Shaft tilting vibration and blade out-of-plane vibration with nodal diameter $k=1$

The blade-shaft coupled torsional vibration that has been commonly taken into account in design [3]-[6] corresponds to ① above, whereas coupled bending vibration occurs under conditions ③ and ④ above. Some reports have been published, but they focus on natural frequency [7]-[9] and the study of blade-shaft vibration control in the case of the external excitation [10]-[11]. These reports do not discuss on coupled resonance in the case of the external excitation. Therefore, this paper discusses the response to the external excitation in the blade-shaft coupled bending vibration under condition ③.

Analysis of the coupling of blade in-plane vibration having nodal diameter $k=1$ with shaft translation motion is given below. More specifically, the existence of an unstable region due to coupling and the characteristics of coupled resonance in an eight-blade ($N=8$) where each blade is assumed to be a 1-DOF mass-spring system, are indicated. The validity of the analysis of coupled resonance is confirmed by experimental data.

2. The Equation of Motion with A Single Blade

This paper considers the blade-shaft coupled bending vibration of an eight-blade ($N=8$) system depicted in Figure 1, where m_s is the mass of the shaft, x_r, y_r are displacements of the shaft in a rotating coordinate system, m is the equivalent mass of the single blade, u_i is displacement in the radial direction and v_i is displacement in the tangential direction of the $\#i$ blade in a rotating coordinate system ($i = 0$ to 7).

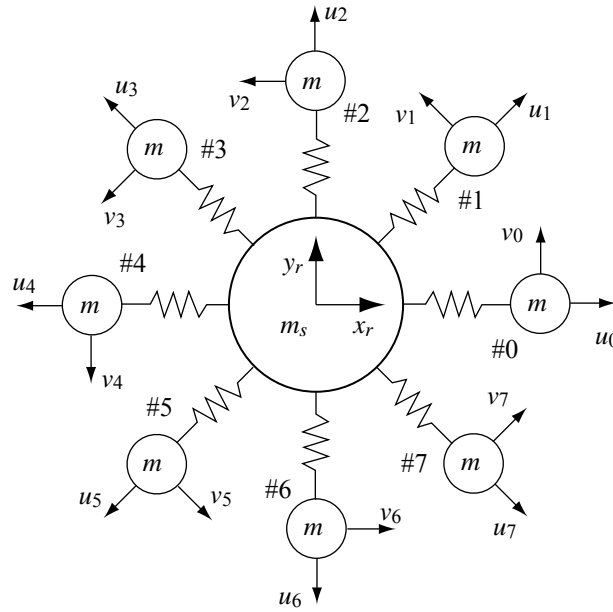


Fig.1 $N=8$ Blade-shaft coupled vibration model

The equation of motion of a single blade is obtained by using Lagrangian equations considering the coupled vibration of the shaft and blades. As shown in Figure 2, rotating coordinate $\{X_r, Y_r, Z_r\}$ is defined as based on the $\#0$ blade which rotates Ωt (rad) centered on fixed coordinate $\{X_0, Y_0, Z_0\}$. The new coordinate $\{X_i, Y_i, Z_i\}$ is defined as based on $\#i$ blade which rotates τ_i at the coordinate $\{X_r, Y_r, Z_r\}$. When the blade vibration displacements are $\{u_i, v_i, 0\}$, the position of the $\#i$ blade tip is $\{r + u_i, v_i, 0\}$ at the coordinate $\{X_i, Y_i, Z_i\}$. The transformation is defined as follows:

$$\mathbf{e}_0 = \mathbf{e}_1 \begin{bmatrix} \cos\theta & \sin\theta & 0 \\ -\sin\theta & \cos\theta & 0 \\ 0 & 0 & 1 \end{bmatrix} \equiv \mathbf{e}_1 \mathbf{T}_3(\theta) \quad (1)$$

Where \mathbf{e}_0 is the unit vector from the fixed coordinate $\{X_0, Y_0, Z_0\}$, and \mathbf{e}_1 is the unit vector in the coordinate system which rotates θ with respect to the Z_0 axis.

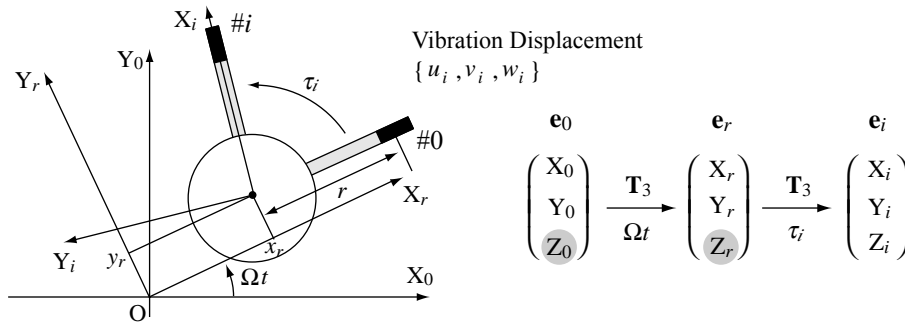


Fig.2 Coordinate system and unit vector

From eq.(1), the position ‘‘P’’ of blade tip from the origin ‘‘O’’ in the fixed coordinate system is expressed as follows:

$$OP = \mathbf{e}_0 \left\{ \mathbf{T}_3^t(\Omega t) \begin{bmatrix} x_r \\ y_r \\ 0 \end{bmatrix} + \mathbf{T}_3^t(\tau_i) \begin{bmatrix} r + u_i \\ v_i \\ 0 \end{bmatrix} \right\} \quad (2)$$

From this equation, the kinematic energy is obtained and the equation of motion is expressed as follows:

$$m \begin{bmatrix} 1 & 0 & \cos \tau_i & -\sin \tau_i \\ 0 & 1 & \sin \tau_i & \cos \tau_i \\ \cos \tau_i & \sin \tau_i & 1 & 0 \\ -\sin \tau_i & \cos \tau_i & 0 & 1 \end{bmatrix} \begin{bmatrix} \ddot{x}_r \\ \ddot{y}_r \\ \ddot{u}_i \\ \ddot{v}_i \end{bmatrix} + 2m\Omega \begin{bmatrix} 0 & -1 & -\sin \tau_i & -\cos \tau_i \\ 1 & 0 & \cos \tau_i & -\sin \tau_i \\ \sin \tau_i & -\cos \tau_i & 0 & -1 \\ \cos \tau_i & \sin \tau_i & 1 & 0 \end{bmatrix} \begin{bmatrix} \dot{x}_r \\ \dot{y}_r \\ \dot{u}_i \\ \dot{v}_i \end{bmatrix} - m\Omega^2 \begin{bmatrix} 1 & 0 & \cos \tau_i & -\sin \tau_i \\ 0 & 1 & \sin \tau_i & \cos \tau_i \\ \cos \tau_i & \sin \tau_i & 1 & 0 \\ -\sin \tau_i & \cos \tau_i & 0 & 1 \end{bmatrix} \begin{bmatrix} x_r \\ y_r \\ u_i \\ v_i \end{bmatrix} = \mathbf{0} \quad (3)$$

3. Mode Synthesis Model for An Eight-Blade System (N=8)

We assume the radial direction displacement $u_i = 0$ due to the radial direction stiffness being significantly larger than tangential direction stiffness. The equation of motion of an eight-blade system is given by the following:

$$m \begin{bmatrix} 8 & 0 & -\mathbf{1}_s^t \\ 0 & 8 & \mathbf{1}_c^t \\ -\mathbf{1}_s & \mathbf{1}_c & \mathbf{E}_8 \end{bmatrix} \begin{bmatrix} \ddot{x}_r \\ \ddot{y}_r \\ \ddot{v} \end{bmatrix} + 2m\Omega \begin{bmatrix} 0 & -8 & -\mathbf{1}_c^t \\ 8 & 0 & -\mathbf{1}_s^t \\ \mathbf{1}_c & \mathbf{1}_s & \mathbf{E}_8 \end{bmatrix} \begin{bmatrix} \dot{x}_r \\ \dot{y}_r \\ \dot{v} \end{bmatrix} - m\Omega^2 \begin{bmatrix} 8 & 0 & -\mathbf{1}_s^t \\ 0 & 8 & \mathbf{1}_c^t \\ -\mathbf{1}_s & \mathbf{1}_c & \mathbf{E}_8 \end{bmatrix} \begin{bmatrix} x_r \\ y_r \\ v \end{bmatrix} = \mathbf{0} \quad (4)$$

where $\mathbf{1}_c^t = [\dots \cos(2\pi(i-1)/N) \dots] = [1 \ 1/\sqrt{2} \ 0 \ -1/\sqrt{2} \ \dots \ 1/\sqrt{2}]$
 $\mathbf{1}_s^t = [\dots \sin(2\pi(i-1)/N) \dots] = [0 \ 1/\sqrt{2} \ 1 \ 1/\sqrt{2} \ \dots \ -1/\sqrt{2}]$
 \mathbf{E}_8 =8-dimensional unit matrix
 $\mathbf{v}^t = [v_0 \ v_1 \ \dots \ v_7]$

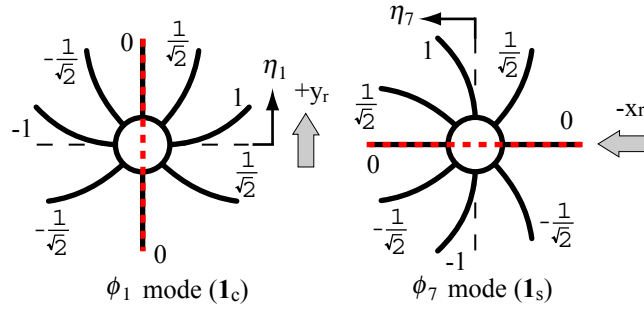


Fig.3 Mode shapes

Figure 3 shows two different modes in blade-shaft coupled bending vibration with nodal diameter $k=1$. The transformation matrix Ψ for mode synthesis containing these modes is given by:

$$\begin{bmatrix} x_r \\ y_r \\ v \end{bmatrix} = \Psi \begin{bmatrix} x_r \\ y_r \\ \eta_1 \\ \eta_7 \end{bmatrix} = \begin{bmatrix} 1 & 0 & 0 & 0 \\ 0 & 1 & 0 & 0 \\ \mathbf{0} & \mathbf{0} & \mathbf{1}_c & -\mathbf{1}_s \end{bmatrix} \begin{bmatrix} x_r \\ y_r \\ \eta_1 \\ \eta_7 \end{bmatrix} \quad (5)$$

and x_r, y_r represent the shaft vibrational displacement, and η_1, η_7 represent the relative blade vibrational displacement in the rotating coordinate system.

The mode synthesis model obtained from the above equation is represented by:

$$\begin{bmatrix} 8m & 4m \\ 4m & 4m \end{bmatrix} \begin{bmatrix} \ddot{x}_r \\ \ddot{y}_r \end{bmatrix} - \Omega \begin{bmatrix} 16m & 8m \\ 8m & 0 \end{bmatrix} \begin{bmatrix} \dot{y}_r \\ \dot{\eta}_1 \end{bmatrix} - \Omega^2 \begin{bmatrix} 8m & 4m \\ 4m & 4m \end{bmatrix} \begin{bmatrix} x_r \\ \eta_7 \end{bmatrix} = \mathbf{0} \quad (6)$$

$$\begin{bmatrix} 8m & 4m \\ 4m & 4m \end{bmatrix} \begin{bmatrix} \ddot{y}_r \\ \ddot{\eta}_1 \end{bmatrix} + \Omega \begin{bmatrix} 16m & 8m \\ 8m & 0 \end{bmatrix} \begin{bmatrix} \dot{x}_r \\ \dot{\eta}_7 \end{bmatrix} - \Omega^2 \begin{bmatrix} 8m & 4m \\ 4m & 4m \end{bmatrix} \begin{bmatrix} y_r \\ \eta_1 \end{bmatrix} = \mathbf{0} \quad (7)$$

Introducing the complex displacements:

$$z_r = x_r + jy_r, \quad \eta_r = \eta_7 + j\eta_1 \quad (8)$$

Equations (6) and (7) can be written as:

$$\begin{bmatrix} 8m & 4m \\ 4m & 4m \end{bmatrix} \begin{bmatrix} \ddot{z}_r \\ \ddot{\eta}_r \end{bmatrix} + j\Omega \begin{bmatrix} 16m & 8m \\ 8m & 0 \end{bmatrix} \begin{bmatrix} \dot{z}_r \\ \dot{\eta}_r \end{bmatrix} - \Omega^2 \begin{bmatrix} 8m & 4m \\ 4m & 4m \end{bmatrix} \begin{bmatrix} z_r \\ \eta_r \end{bmatrix} = \mathbf{0} \quad (9)$$

We assume here that the natural frequency ω_b of the blade in the tangential direction is given by Finite Element Method (FEM) vibration analysis that takes into account the centrifugal stiffness during rotation. Representing the overall tangential stiffness as $k_b = m\omega_b^2$ and substituting k_b for the (2,2) element of the stiffness matrix in Eq. (9) above, we obtain:

$$\begin{bmatrix} 8m & 4m \\ 4m & 4m \end{bmatrix} \begin{bmatrix} \ddot{z}_r \\ \ddot{\eta}_r \end{bmatrix} + j\Omega \begin{bmatrix} 16m & 8m \\ 8m & 0 \end{bmatrix} \begin{bmatrix} \dot{z}_r \\ \dot{\eta}_r \end{bmatrix} + \begin{bmatrix} -8m\Omega^2 & -4m\Omega^2 \\ -4m\Omega^2 & 4k_b \end{bmatrix} \begin{bmatrix} z_r \\ \eta_r \end{bmatrix} = \mathbf{0} \quad (10)$$

For observation of the blade vibration from a fixed coordinate, we rewrite Eq. (10) for a fixed coordinate system by making displacement z and η correspond to z_r and η_r using:

$$z = z_r e^{j\Omega t}, \quad \eta = \eta_r e^{j\Omega t} \quad (11)$$

Resulting in:

$$\begin{bmatrix} 8m & 4m \\ 4m & 4m \end{bmatrix} \begin{bmatrix} \ddot{z} \\ \ddot{\eta} \end{bmatrix} + j\Omega \begin{bmatrix} 0 & 0 \\ 0 & -8m \end{bmatrix} \begin{bmatrix} \dot{z} \\ \dot{\eta} \end{bmatrix} + \begin{bmatrix} 0 & 0 \\ 0 & 4k_b - 4m\Omega^2 \end{bmatrix} \begin{bmatrix} z \\ \eta \end{bmatrix} = \mathbf{0} \quad (12)$$

Finally, superimposing shaft mass m_s and the spring constant k_s of the shaft in the direction of parallel motion into Eq. (12) leads to the mode synthesis model.

$$\begin{bmatrix} m_s + 8m & 4m \\ 4m & 4m \end{bmatrix} \begin{bmatrix} \ddot{z} \\ \ddot{\eta} \end{bmatrix} + j\Omega \begin{bmatrix} 0 & 0 \\ 0 & -8m \end{bmatrix} \begin{bmatrix} \dot{z} \\ \dot{\eta} \end{bmatrix} + \begin{bmatrix} k_s & 0 \\ 0 & 4k_b - 4m\Omega^2 \end{bmatrix} \begin{bmatrix} z \\ \eta \end{bmatrix} = \mathbf{0} \quad (13)$$

4. Equivalent Mass of The Shaft with Rigid Blades

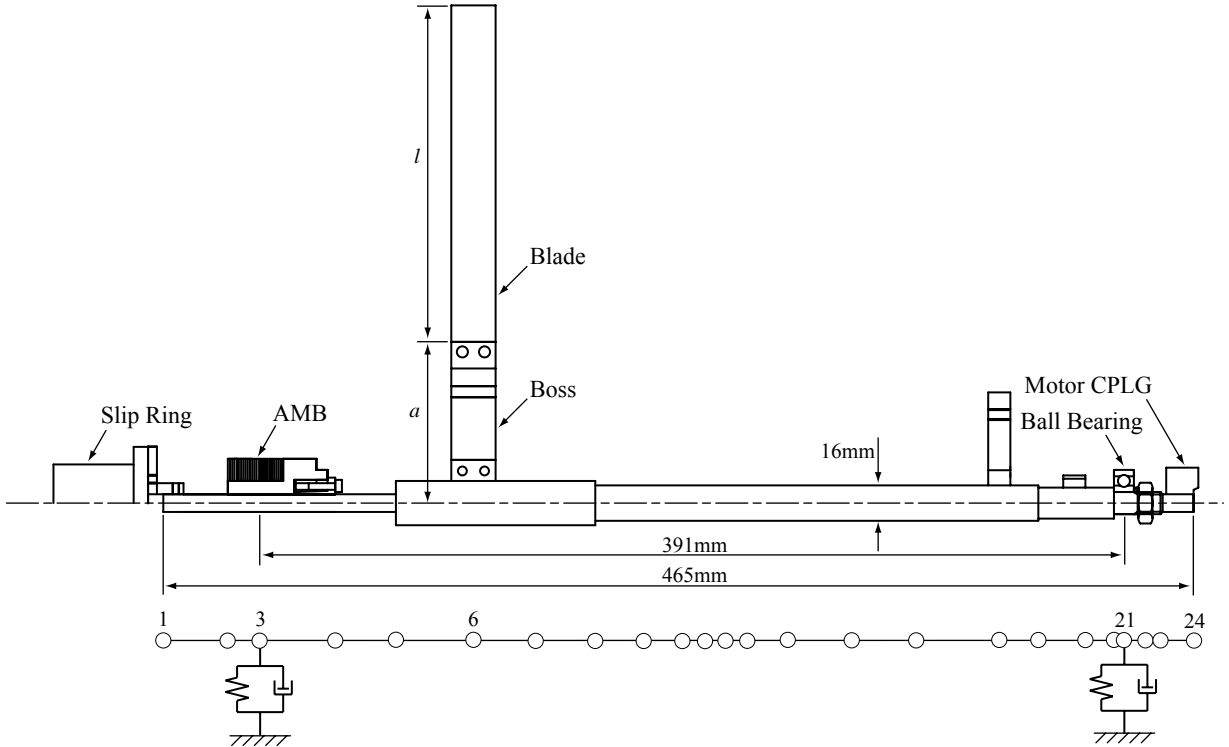


Fig.4 Finite element method model

The equivalent mass of the shaft with rigid blades is calculated in order to obtain the shaft reduction model. An FEM model is constructed by dividing the axis shown in Figure 4 by 24 nodal points. Nodal point 3 corresponds to the Active Magnetic Bearing (AMB), point 6 to the boss with the rigid blade, and point 21 to the ball bearing.

Figure 5 shows the static deflection mode of the FEM model by forced displacement of the nodal point for AMB.

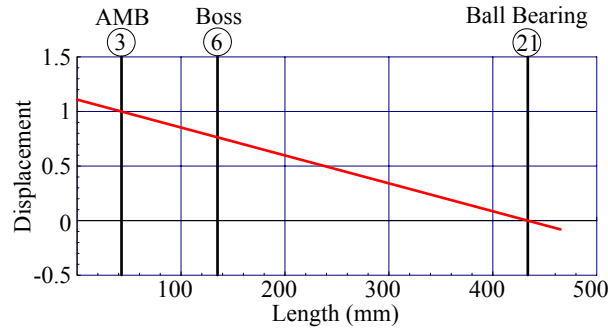


Fig.5 Deflection mode of the FEM model

Fig.5 gives the displacement of the nodal point for the boss with rigid blade of 0.782 for a displacement by 1 of the AMB nodal point. We now proceed to the 5-dof mode-synthesis model with the AMB and ball bearing as the boundary coordinates, taking into account the internal system mode up to the third order.

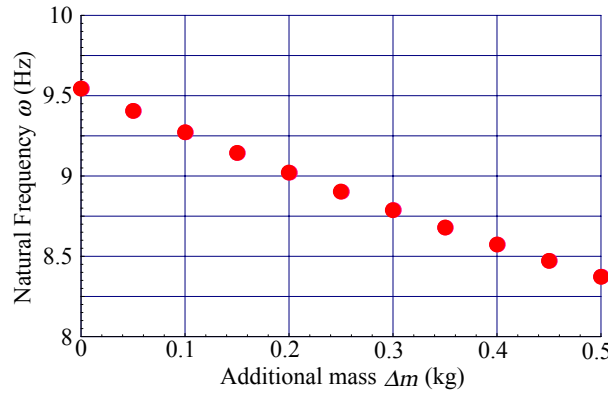


Fig.6 The natural frequency with an additional mass

Figure 6 shows the natural frequency calculated for the model with an additional mass Δm at the position of the AMB. Natural frequency without additional mass $f_0=9.69\text{Hz}$ and a gradient $\alpha=2.46$ can be read from Fig.6. The method of Oyama et al. [12] enables us to obtain the modal equivalent mass m_{eq} of the nodal point for the boss with rigid blade as follows:

$$m_{eq} = \frac{f_0}{2\alpha} \left(\frac{1}{0.782} \right)^2 = 3.2\text{kg} \quad (14)$$

5. Blade-Shaft Coupled Model with Two Degrees of Freedom

In correspondence to the experiment described later, we represent shaft vibration in terms of displacement z in a fixed coordinate system, corresponding to the reading of the displacement pick-up. The blade vibration is described in terms of displacement η_r in a rotating coordinate system, corresponding to the reading of the strain gauge. The relationship between the two coordinate systems is shown by Eq. (11). Thus, Eq. (13) is rewritten as:

$$(m_s + 8m)\ddot{z} + 4m \frac{d^2}{dt^2} (\eta_r e^{j\Omega t}) + k_s z = 0 \quad (15)$$

$$4m\ddot{z} e^{-j\Omega t} + 4m\ddot{\eta}_r + 4k_b \eta_r = 0 \quad (16)$$

These formulas can be simplified by defining the following variables.

$$\omega_s = \sqrt{k_s / (m_s + 8m)} = \text{Shaft natural frequency of the system}$$

(in a fixed coordinate system, not coupled; assuming the blade as a rigid body)

$$\omega_b = \sqrt{k_b / m} = \text{Blade natural frequency (in a rotating coordinate system, not coupled; assuming the shaft as fixed)}$$

$$\mu = 4m / (m_s + 8m) = (\text{equivalent mass of blades}) / (\text{equivalent mass of the shaft with rigid blades } m_{eq}) = \text{mass ratio}$$

When considering centrifugal effects, blade natural frequency is calculated by:

$$\omega_b^2 = \omega_{b0}^2 + C\Omega^2 \quad (17)$$

Where, ω_{b0} = Blade natural frequency without rotation
 $C = 1 + 1.45 a/l - \cos^2 \theta_0$ = Centrifugal Coefficient [13]
 a = Radius of the boss
 l = Blade length
 θ_0 = Stagger angle

These variables permit rewriting Eqs. (15) and (16) to give the below equations of motion for the blade-shaft coupled model.

$$\ddot{z} + \omega_s^2 z + \mu \frac{d^2}{dt^2} (\eta_r e^{j\Omega t}) = 0 \quad (18)$$

$$\ddot{z} e^{-j\Omega t} + \ddot{\eta}_r + \omega_b^2 \eta_r = 0 \quad (19)$$

If the damping ratio of the shaft and the blade ζ_s, ζ_b are considered, and an external harmonic force $f(t) = e^{j\nu t}$ is whirling excitation, ν being the excitation frequency of whirl, the equations of motion become:

$$\ddot{z} + 2\zeta_s \omega_s \dot{z} + \omega_s^2 z + \mu \frac{d^2}{dt^2} (\eta_r e^{j\Omega t}) = e^{j\nu t} \quad (20)$$

$$\ddot{z} e^{-j\Omega t} + \ddot{\eta}_r + 2\zeta_b \omega_b \dot{\eta}_r + \omega_b^2 \eta_r = 0 \quad (21)$$

6. Coupled Resonance and Stability

6.1 Free vibration solution for an undamped system

Considering that the natural frequency ω as viewed from a fixed coordinate can be converted to ω_r as viewed from a rotating coordinate by:

$$\omega_r = \omega - \Omega \quad (22)$$

The solutions of Eqs. (18) and (19) can be written as:

$$z = A e^{j\omega t}, \quad \eta_r = B e^{j(\omega - \Omega)t} \quad (23)$$

Substituting Eq.(23) into Eqs. (18) and (19) yields the characteristic equation:

$$\begin{vmatrix} -\omega^2 + \omega_s^2 & -\mu \omega^2 \\ -\omega^2 & -(\omega - \Omega)^2 + \omega_b^2 \end{vmatrix} = 0 \quad (24)$$

The undamped natural frequency ω (for a fixed coordinate system) was obtained from Eq. (24). Figure 7 shows the results for $\omega_s = 8.0$ Hz, $\omega_{b0} = 21.5$ Hz, $\mu = 0.067$, and $C = 0$, where \mathbf{e}_0 indicates presentation in a fixed coordinate system and \mathbf{e}_r in a rotating coordinate system.

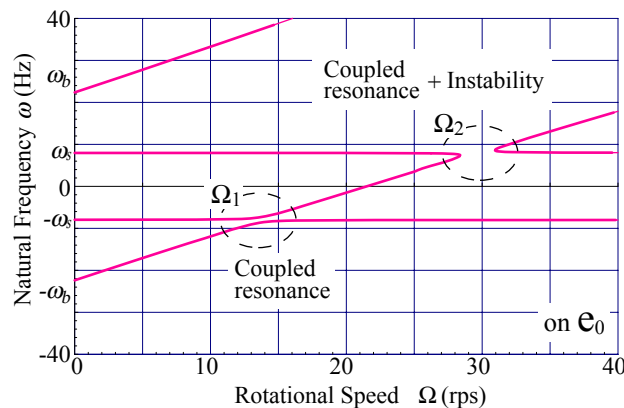


Fig.7 Eigenvalue map
 $(\omega_s = 8.0\text{Hz}, \omega_{b0} = 21.5\text{Hz}, \mu = 0.067, C = 0)$

Fig. 7 shows the representation in a fixed coordinate system with rotational speed Ω (rps) on the horizontal axis and natural frequency ω (Hz) on the vertical axis. The natural frequency of the blade and that of the shaft are widely separated from each other when $\Omega = 0$ rps (at rest), but they become closer as the rotational speed increases. The two curves come very close to each other and then separate (“near-miss”) [9] when the difference between the two natural frequencies is around $\Omega_1 = |\omega_s - \omega_b| = 13.5$ rps.

This indicates blade-shaft coupling. Two natural frequency curves come close again and the two curves are broken at around $\Omega_2 = \omega_s + \omega_b = 29.5$ rps, where eigenvalues change to complex numbers with positive real parts, the region represents an unstable region of the undamping system.

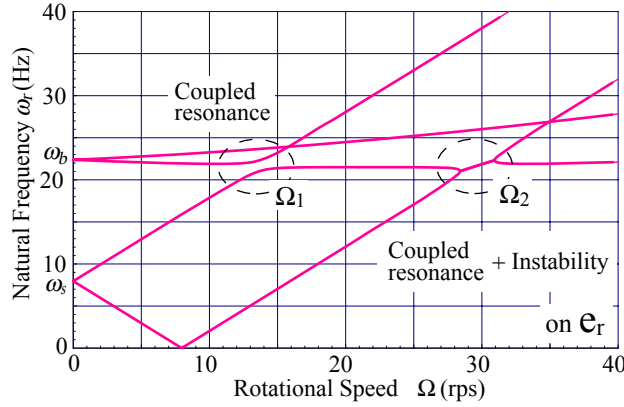


Fig.8 Eigenvalue map
 ($\omega_s = 8.0$ Hz, $\omega_{b0} = 21.5$ Hz, $\mu = 0.067$, $C = 0$)

Figure 8 represents the absolute values of the undamped natural frequencies ω_r (for a rotating coordinate system) obtained from Eqs. (22) and (24) in a rotating coordinate system. As in Fig. 7, the parameters are $\omega_s = 8.0$ Hz, $\omega_{b0} = 21.5$ Hz, $\mu = 0.067$, and $C = 0$; the horizontal axis represents rotational speed Ω (rps) and the vertical axis the natural frequency ω_r (Hz). Each blade and shaft has a single natural frequency at $\Omega = 0$ rps, which is split into a forward and backward natural frequency at higher rotational speeds. Blade-shaft coupling occurs at around $\Omega_1 = |\omega_s - \omega_b| = 13.5$ rps, separating the two natural frequency curves. Further increase in the rotational speed leads to a second blade-shaft coupling at around $\Omega_2 = \omega_s + \omega_b = 29.5$ rps. The curves are not broken as in Fig.7 when they approach Ω_2 because Fig.8 shows the absolute values of the undamped natural frequency ω_r , although an unstable region does exist.

6.2 Effects of centrifugal force

The natural frequency ω_b of the blade actually increases with the rotational speed Ω because of centrifugal force. Figures 9 and 10 show the undamped natural frequencies ω (for a fixed coordinate system) and ω_r (for a rotating coordinate system), respectively, obtained from the blade natural frequency ω_b calculated for $\omega_s = 8.0$ Hz, $\omega_{b0} = 21.5$ Hz, $\mu = 0.067$, and $C = 0.7$.

Because of the natural frequency ω_b of the blade bending with centrifugal effect, blade-shaft coupled rotational speeds Ω_1 and Ω_2 as seen from Figs. 9 and 10, move to the high rotational speed side as compared with Figs. 7 and 8: $\Omega_1 = |\omega_s - \omega_b|$ is around 20 rps and $\Omega_2 = \omega_s + \omega_b$ is around 70 rps.

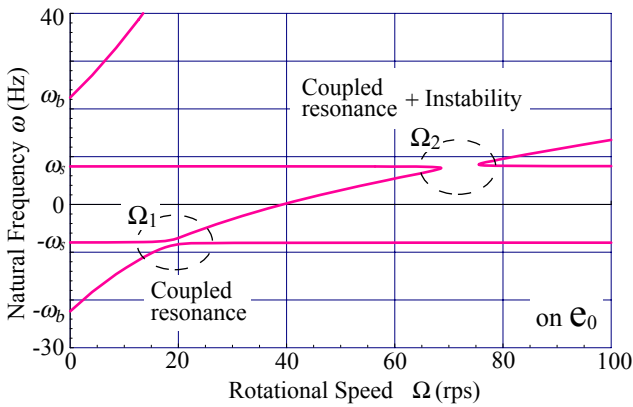


Fig.9 Eigenvalue map
 ($\omega_s = 8.0$ Hz, $\omega_{b0} = 21.5$ Hz, $\mu = 0.067$, $C = 0.7$)

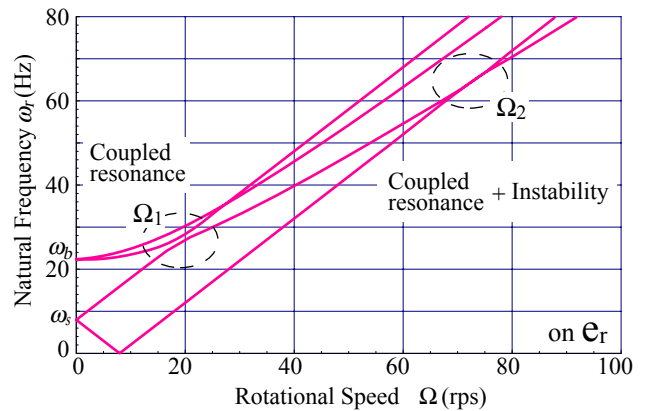


Fig.10 Eigenvalue map
 ($\omega_s = 8.0$ Hz, $\omega_{b0} = 21.5$ Hz, $\mu = 0.067$, $C = 0.7$)

6.3 Stabilization

The free vibration solutions of Eqs. (20) and (21) for the external force = 0 may be written in the following forms.

$$z = A e^{st}, \quad \eta_r = B e^{(s-j\Omega)t} \tag{25}$$

Substituting Eq. (25) into Eqs. (20) and (21) gives a characteristic equation:

$$\begin{bmatrix} s^2 + 2\zeta_s \omega_s s + \omega_s^2 & \mu s^2 \\ s^2 & (s - j\Omega)^2 + 2\zeta_b \omega_b (s - j\Omega) + \omega_b^2 \end{bmatrix} \begin{bmatrix} A \\ B \end{bmatrix} = \mathbf{0} \quad (26)$$

Analysis of complex eigenvalues at $\Omega=0, 20$ and 70 rps, with values of the damping ratio $\zeta_s=0.04$ and $\zeta_b=0.008$, gives results shown in Table2.

Table2 Complex eigenvalue analysis

Rotational Speed (rps)	Natural Frequency (Hz / Hz)	Damping Ratio	Q-factor
$\Omega=0$	8.0/-8.0 22.4/-22.4	0.039 / 0.039 0.010 / 0.010	13 / 13 52 / 52
$\Omega_1=20$	8.0 / -8.3 50 / -7.0	0.040 / 0.040 0.030 / 0.006	13 / 12 16 / 87
$\Omega_2=70$	7.9 / -8.0 143 / -7.7	0.011 / 0.040 0.094 / 0.004	47 / 12 5.3 / 114

The natural frequency curves are no longer broken here because the results indicate that the system is stable at $\Omega_2 = \omega_s + \omega_b = 70$ rps. However, a very high value of the Q-factor suggests a significant coupled resonance.

Although we do not show the details here, the stabilization requires a damping ratio satisfying the following condition:

$$\sqrt{\zeta_s \zeta_b} > \frac{\sqrt{\mu} \omega_s}{2 \omega_b} \quad (27)$$

Eq. (27) shows that the greater the mass ratio μ , the greater the damping needed for stabilization.

6.4 Response to whirling excitation of the shaft

When the external force in Eq. (20) is whirling excitation of the shaft (forward when $\nu > 0$, backward when $\nu < 0$), the forced vibration solution may be written as:

$$z = A e^{j\nu t}, \quad \eta_r = B e^{j(\nu - \Omega)t} \quad (28)$$

Substituting Eq. (28) into Eqs. (20) and (21) gives an equation for the amplitude:

$$\begin{bmatrix} -\nu^2 + j2\zeta_s \omega_s \nu + \omega_s^2 & -\mu \nu^2 \\ -\nu^2 & -(\nu - \Omega)^2 + j2\zeta_b \omega_b (\nu - \Omega) + \omega_b^2 \end{bmatrix} \begin{bmatrix} A \\ B \end{bmatrix} = \begin{bmatrix} 1 \\ 0 \end{bmatrix} \quad (29)$$

The amplitude of the coupled vibration of the shaft and blades was calculated by assigning the same parameter values as above to the relevant variables in Eq. (29) for both forward and backward excitation.

Figure 11 shows resonance curves at different rotational speeds ($\Omega=0, 10, 20, 50, 70$ rps) for forward and backward excitation by plotting the shaft and blade vibration in fixed coordinates.

For $\Omega=0$ rps (at rest), the peak of shaft vibration appears at ± 8 Hz (a and a' in Fig. 11), corresponding to the natural frequency ω_s of the shaft. Blade vibration shows a peak at ± 21.5 Hz (b and b' in Fig. 11) and weak resonance ± 8 Hz (c and c' in Fig. 11), corresponding to the natural frequency ω_b of the blade and the natural frequency of the shaft, respectively.

For higher rotational speeds, the blade vibration peak shifts from -21.5 Hz ($-\omega_b$) toward higher frequencies, and coincides at $\Omega=20$ rps (corresponding to $\Omega_1 = |\omega_s - \omega_b|$) with the natural frequency of the shaft $-\omega_s = -8$ Hz. Here, the blades act as dynamic vibration absorbers of shaft vibration, resulting in an anti-resonance point appearing in shaft vibration (d in Fig. 11) which is limited to a relatively small amplitude, whereas the blades show a relatively large resonance (e in Fig. 11).

When the rotational speed further increases to $\Omega=70$ rps corresponding to $\Omega_2 = \omega_s + \omega_b$, the blade vibration peak shifts from -21.5 Hz ($-\omega_b$) coincides with the natural frequency of the shaft $+\omega_s = +8$ Hz. No anti-resonance point appears in this case; a violent blade-shaft coupled resonance occurs with a very large amplitude (f and g in Fig. 11).

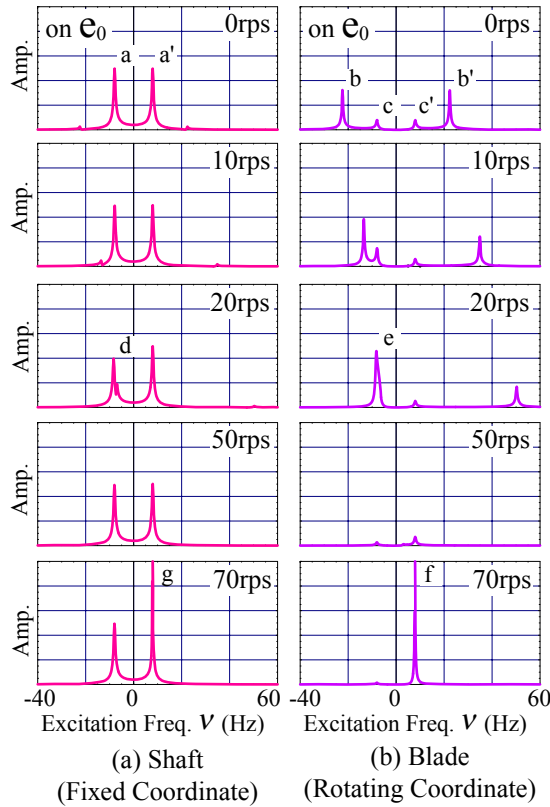


Fig.11 Resonance curve
 $(\omega_s = 8.0\text{Hz}, \omega_{b0} = 21.5\text{Hz}, \mu = 0.067, C = 0.7)$

Figure 12 shows waterfall diagrams for the blade-shaft resonance under forward and backward excitation. The curves represent the amplitudes as functions of the frequency ν (Hz) of the shaft whirling excitation and rotational speed plotted in a fixed coordinate system. The blade-shaft coupling around $\Omega_1 = |\omega_s - \omega_b| = 20\text{rps}$ leads to increased blade vibration and a relatively weak shaft vibration peaks split below and above an anti-resonance point. The curves clearly show a violent coupled resonance and increasing vibration around $\Omega_2 = \omega_s + \omega_b = 70\text{rps}$.

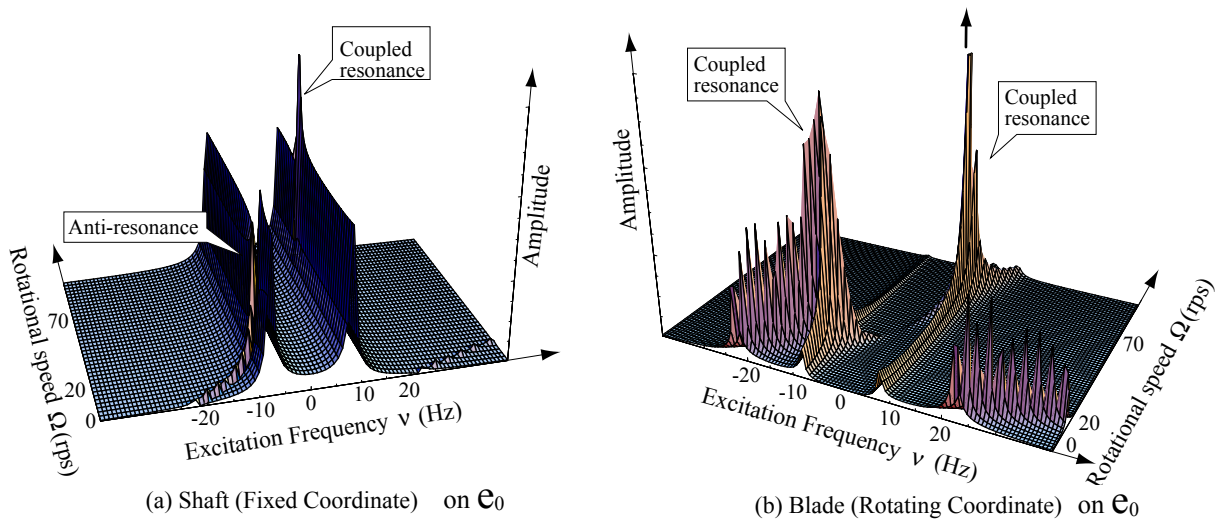


Fig.12 Waterfall diagram
 $(\omega_s = 8.0\text{Hz}, \omega_{b0} = 21.5\text{Hz}, \mu = 0.067, C = 0.7)$

7. Experiment

A test rig was configured as shown in the diagram of Figure 13 and photograph of Figure 14. A self-made rotor with blades was mounted on a rotating shaft supported by a ball bearing at the left end and by an Active Magnetic Bearing (AMB) at the right end. A 1,200-watt AC servo motor (UNICO JAPAN) was used to drive the shaft. The rotor was provided with eight flat blades

arranged equidistantly at stagger angle $\theta_0 = 0$ deg. A weight affixed at each blade tip permits adjustment of the natural frequency ω_{b0} of the blade.

In an experimental run, the shaft was excited vertically via the AMB while the rotating speed was increased gradually. The frequency of the excitation ν was 8.0 Hz which corresponds to the natural frequency of the shaft ω_s . The shaft vibration was measured with eddy-current-type displacement pickups (for X and Y) attached to the AMB, and the vibration of the blade with a strain gauge attached to the root of the blade. The results were analyzed using FFT. The experimental conditions and parameters were as follows.

Total weight: 2.6 kg
 Shaft length: 0.465 m
 Number of blades: $N=8$
 Blade length: 0.152 m
 Weight added to the blade: 0.044 kg

Stagger angle: $\theta_0 = 0$ deg.
 Natural frequency of the blade: $\omega_{b0} = 21.5$ Hz
 Natural frequency of the shaft: $\omega_s = 8.0$ Hz (in the first mode)
 Measurement range of rotational speed: $\Omega = 0$ to 30 rps
 Excitation frequency: $\nu = 8.0$ Hz

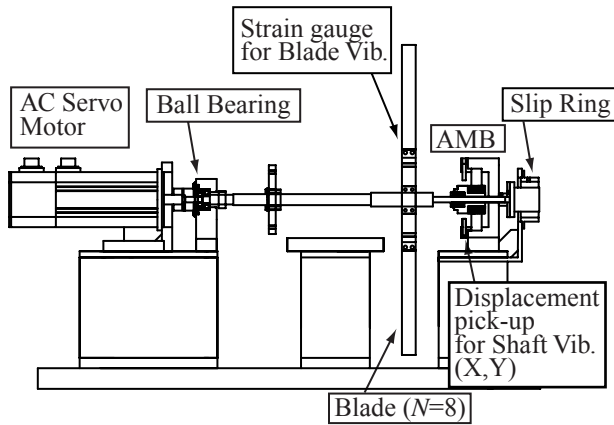


Fig.13 Test rig

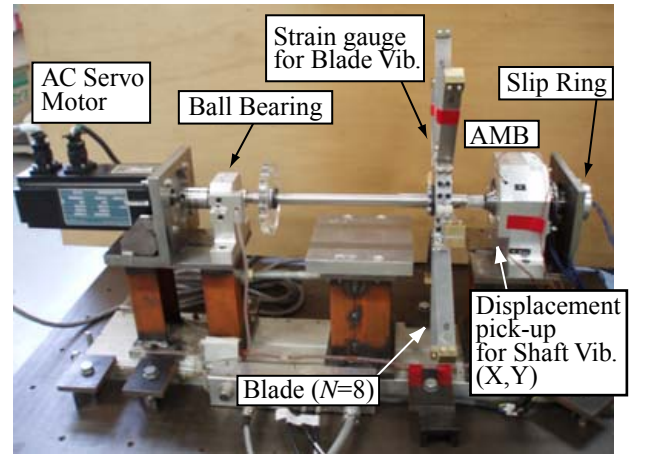


Fig.14 Photograph of the test rig

Figure 15, which is zoomed in Fig.10, shows the experimental values of the blade natural frequency as dots for comparison with the ω_r values calculated from Eq. (24), which are represented by solid lines. The close agreement between the observed data and the calculated blade natural frequency $|\pm\omega_b|$ taking the centrifugal force into account confirm the validity of the latter.

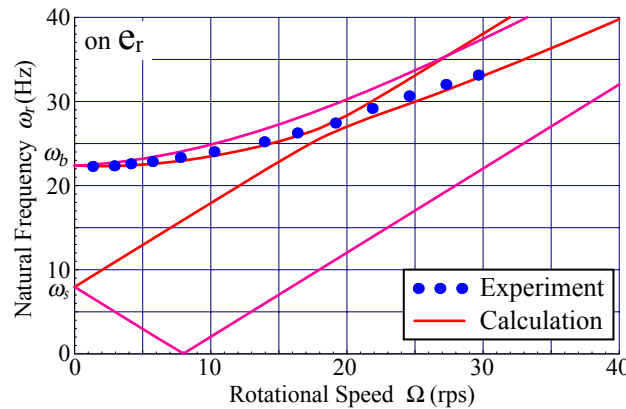


Fig.15 Blade natural frequency
 ($\omega_s = 8.0$ Hz, $\omega_{b0} = 21.5$ Hz, $\mu = 0.067$, $C = 0.7$)

Figure 16 shows blade vibration as measured by a strain gauge on a Campbell diagram. The rotational speed Ω is on the horizontal axis and the observed frequency of the blade vibration on the vertical axis. Amplitude is represented by the diameter of the circle. The large vibration in the 1X component is caused by excited blades with gravity, and falls outside the scope of the present paper.

The Campbell diagram is used to represent a rotating coordinate system because the data was obtained by the strain gauge attached to a blade. For clarity, the blade natural frequency ω_b observed is shown by dotted lines in the diagram, and clearly increases with increasing rotational speed Ω under the influence of centrifugal force. The excitation of the shaft in the vertical direction (in a fixed coordinate system) at $\nu = 8.0$ Hz is represented by the forward natural frequency $+\omega_s = +8.0$ Hz and the backward frequency $-\omega_s = -8.0$ Hz, both being independent of the rotational speed. However, they depend on the rotational speed in the representation in a rotating coordinate system, as shown by the dotted lines in the figure: the forward $|+\omega_s - \Omega|$ and the

backward $|\omega_s - \Omega|$. The figure shows that the backward natural frequency $|\omega_s - \Omega|$ approaches the blade natural frequency ω_b in the vicinity of $\Omega_1 = |\omega_s - \omega_b| = 20$ rps, where the amplitude is greater than at other rotational speeds.

This experiment visualized the blade vibration increase by the blade-shaft coupling at a rotational speed around $\Omega_1 = |\omega_s - \omega_b| = 20$ rps, as calculated by simulation. However, the other coupling at around $\Omega_2 = \omega_s + \omega_b = 70$ rps was not observed due to the rotational speed limit of 30 rps in the present test rig.

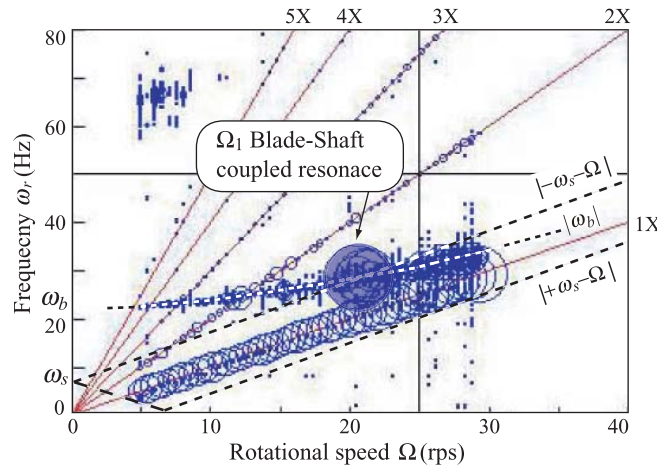


Fig.16 Campbell diagram with blade vibration
($\omega_s = 8.0\text{Hz}$, $\omega_{b0} = 21.5\text{Hz}$, In-plane)

8. Conclusion

Analysis of coupling of the translation shaft-radial vibration mode with in-plane vibration of the blade with nodal diameter $k = 1$ yielded the following results.

- (1) A mode synthesis model was presented for vibration of an eight-blade system ($N=8$, nodal diameter $k=1$) and vibration of the shaft.
- (2) The equations of motion for the blade and shaft were used for analyzing coupled free vibration. The natural frequency curves separated from each other at a rotational speed $\Omega_1 = |\omega_s - \omega_b|$, and were broken at $\Omega_2 = \omega_s + \omega_b$, indicating an unstable region. Stabilization by damping eliminates the breakage at Ω_2 , but complex eigenvalue analysis resulted in a very high Q-factor.
- (3) Simulation of forced vibration of a stable damping system showed that, at $\Omega_1 = |\omega_s - \omega_b|$, shaft vibration is relatively weak due to anti-resonance points resulting from the dynamic vibration absorber effect of the blades, whereas a significant resonance occurs in the blades. Meanwhile, a violent coupled resonance occurs at $\Omega_2 = \omega_s + \omega_b$.
- (4) The resonance in blade vibration at $\Omega_1 = |\omega_s - \omega_b|$ described in (3) was experimentally confirmed.

Acknowledgments

The authors would like to express their heartfelt gratitude for the support provided by UNICO JAPAN CO.,LTD.

Nomenclature

N	Number of blades	m_{eq}	Equivalent mass of the shaft with rigid blades [kg]
m_s	Mass of the shaft [kg]	ω_s	Shaft natural frequency [Hz]
m	Equivalent mass of a single blade [kg]	ω_b	Blade natural frequency [Hz]
k_s	Spring constant of the shaft [N/m]	ω_{b0}	Blade natural frequency without rotation [Hz]
k_b	Spring constant of a single blade [N/m]	C	Centrifugal Coefficient
ζ_s	Damping ratio of the shaft	θ_0	Stagger angle [deg.]
ζ_b	Damping ratio of a single blade	a	Radius of the boss [m]
x_r, y_r	Shaft displacement in a Rotating coordinate system [m]	l	Blade length [m]
u	Blade displacement in the radial direction [m]	Ω	Rotational speed [rps]
v	Blade displacement in the tangential direction [m]	ν	Whirling excitation frequency of the shaft [Hz]

References

- [1] Shigeo Tanaka, 1997, "Analysis of Blade-Disc Coupled Vibration," Mitsubishi Heavy Industries Technical Review, Vol. 14, No. 2, pp. 134-142.
- [2] Yasumoto Kaneko, Kazushi Mori, Masayuki Tomii, Hiroharu Ohyama, 2006, "Reduction of Resonant Stress of Turbine Blade by Use of Asymmetric Vane Spacing (Effect of Multi-resonance on Reduction of Vibratory Stress)," Transactions of the Japan Society of Mechanical Engineers, Series C, Vol. 72, No. 720, pp. 26-32.
- [3] Osami Matsushita, Toyomi Yoshida, Kiyoshi Namura, Akira Okabe, Ryoichi Kaneko, 1990, "Torsional Vibration Analysis of Turbine-Generator Blade Coupled System," The Thermal and Nuclear Power, Vol. 41, No. 1, pp. 49-56.
- [4] A. Okabe, Y. Otawara, R. Kaneko, O. Matsushita, K. Namura, 1991, "An equivalent reduced modelling method and its application to shaft-blade coupled torsional vibration analysis of a turbine-generator set," IMechE, Vol. 205, pp. 173-181.
- [5] Hiroshi Kanki, Kazuo Tsukuda, 1990, "Reliability Improvement of Blade Rotor Coupled Vibration Using Large Torsional Exciter," Mitsubishi Heavy Industries Technical Review, Vol. 27, No. 1, pp. 1-3.
- [6] Hiroshi Mimuro, Eiji Tshunoda, Hitoshi Sakakida, 1988, "Torsional Vibration Evaluation Technique For Large-Capacity Steam Turbine Generators," Toshiba Review, Vol. 43, No. 4, pp. 369-372.
- [7] Noriaki Hagiwara, Yasuo Ono, Hiroshi Iijima, 1985, "Natural frequencies of forward and backward whirling mode of blades (1st report, Analysis of influences of shaft and rotating effects)," Transactions of the Japan Society of Mechanical Engineers, Series C, Vol. 51, No. 463, pp. 555-564.
- [8] Hiroshi Iijima, Shuji Goto, Noriaki Hagiwara, 1985, "Natural frequencies of forward and backward whirling of blades. 2nd report Experiment by models with flat blades fixed to a shaft in its middle," Transactions of the Japan Society of Mechanical Engineers, Series C, Vol. 51, No. 472, pp. 3228-3234.
- [9] Giancarlo Genta, 2005, Dynamics of Rotating Systems, Springer.
- [10] Santos, I. F., Saracho, C. M., Smith, J. T. and Eiland, J., 2004, "Contribution to Experimental Validation of Linear and Non-Linear Dynamic Models for Representing Rotor-Blades Parametric Coupled Vibrations," Journal of Sound and Vibration, Vol. 271, No. 3, pp. 883-904.
- [11] Christensen, R. H. and Santos, I. F., 2006, "Active Rotor-Blade Control Vibration using Shaft-Based Electro-Magnetic Actuation," ASME Journal of Engineering for Gas Turbine and Power, Vol. 128, pp. 644-652.
- [12] Hiroto Oyama, Norihisa Anegawa, Hiroyuki Fujiwara, Osami Matsushita, 2007, "A method to evaluate eigenvalues of rotor-bearing system using the modal open loop transfer function," The 9th Asian International Conference of Fluid Machinery, No. AICFM9-266.
- [13] The Japan Society of Mechanical Engineers, 2001, Mechanical Engineers' Handbook, Maruzen.